Confocal detection of planar homogeneous and heterogeneous immunosorbent assays

Homanaz Ghafari
Yanzhou Zhou*
Selman Ali
Quentin S. Hanley
Nottingham Trent University
School of Science and Technology
Clifton Lane
Nottingham NG11 8NS
United Kingdom

Abstract. Optically sectioned detection of fluorescence immunoassays using a confocal microscope enables the creation of both homo- and heterogeneous planar format assays. We report a set assays requiring optically sectioned detection using a model system and analysis procedures for separating signals of a surface layer from an overlying solution. A model sandwich assay with human immunoglobulin G as the target antigen is created on a glass substrate. The prepared surfaces are exposed to antigen and a FITC-labeled secondary antibody. The resulting preparations are either read directly to provide a homogeneous assay or after wash steps, giving a heterogeneous assay. The simplicity of the object shapes arising from the planar format makes the decomposition of analyte signals from the thin film bound to the surface and overlayer straightforward. Measured response functions of the thin film and overlayer fit well to the Cauchy-Lorentz and cumulative Cauchy-Lorentz functions, respectively, enabling the film and overlayer to be separated. Under the conditions used, the detection limits for the homogeneous and heterogeneous forms of the assay are 2.2 and 5.5 ng/ml, respectively. Planar format, confocally read fluorescence assays enable wash-free detection of antigens and should be applicable to a wide range of assays involving surface-bound species.
[DOI: 10.1117/1.3268772]

Keywords: confocal laser scanning microscopy; sandwich immunoassay; fluorescence-linked immunosorbent assay; homogenous assay.

Paper 09024RR received Jan. 27, 2009; revised manuscript received Sep. 30, 2009; accepted for publication Oct. 2, 2009; published online Dec. 7, 2009.

1 Introduction

Immunoassay is an analytical technology that has been widely used for diagnosis, chemical analysis, and screening.[1] It is a quantitative assay that depends on the reaction between an antigen and an antibody.[2] Since its origin around 1960 with the introduction of the first generation of radioimmunoassay until the present, research efforts have been directed toward increasing the sensitivity, decreasing the processing time, and reducing the amount of reagents and sample required.[3] A sandwich immunoassay is based on two antibodies that bind to different sites on an antigen. Typically, an enzyme or a fluorophore is attached to the secondary antibody followed by absorbance or fluorescence detection. These techniques are enzyme-linked immunosorbent assay (ELISA) and fluorescence-linked immunosorbent assay (FLISA), respectively.[2]

Immunochemical assay methods can be grouped to heterogeneous and homogeneous formats. Heterogeneous formats require separation of bound and free labels before measuring the results. Homogeneous assays do not require this separation step and therefore tend to be faster, simpler, and more amenable to automation. There is a wide range of homogeneous format assays in the literature. These vary from assays within a single liquid phase followed by turbidimetric,[4] colorimetric,[5–7] fluorometric,[8,9] and luminescent[10] detection schemes to biphasic assays in which reagents partition between a liquid and a solid phase. Examples of the latter include beads,[11–14] colloidal gold and latex particles,[15,16] membranes,[17,18] and cells.[19–21] Some authors have argued that the term homogeneous be restricted to assays where the solid phase remains suspended in solution,[22] however, there is no general agreement on this point. Here we use the term homogeneous to refer to a biphasic assay that does not require separation of free reagents via wash steps.

Confocal laser scanning microscopy (CLSM) is an imaging technique producing optical sections of a 3-D specimen from a single focal plane by introducing illumination and detection pinholes. The optical sections have a shallow depth of field, enabling collection of data from a single plane rather than the entire thickness of the specimen. The elimination of out-of-focus light results in an increase in contrast, clarity, and detection sensitivity.[23] By moving the focal plane along the z axis, a series of optical sections can be recorded. The important advantage of confocal microscopy is the improve-

*Current address: Faculty of Automation, Guangdong University, Guangzhou, Guangdong 510006, P.R. China.

Address all correspondence to: Quentin S. Hanley, Nottingham Trent University, School of Science and Technology, Clifton Lane, Nottingham NG11 8NS, United Kingdom: Tel: 44-0115-848-3536; Fax: 44-0115-848-3384; E-mail: quentin.hanley@ntu.ac.uk

1083-3668/2009/14(6)/064022/10/$25.00 © 2009 SPIE

ment in z axis (axial) resolution due to elimination of out-of-focus photons. Axial resolution depends on the pinhole size, the numerical aperture (NA) of the objective, and the excitation and emission wavelengths. The scan speed of CLSM is limited by its low duty cycle, however, a variety of alternative optical sectioning methods exist, including multipoint[24] (Nipkow-type spinning-disk microscopy) and line scanning laser microscopy[25] (L2M), programmable array microscopy (PAM),[26,27] and spinning disks equipped with a microlens arrays.[28] These and a variety of other structured light approaches[29,30] could provide optical sectioning for fast detection of planar format assays.

Detection of a FLISA by CLSM has been described previously for bead-based assays[11,13,31–33] and spot microarray formats.[34] Although confocal readout has been described in these papers, they were not carried out in a homogeneous planar format nor have the characteristics of the confocal response from these systems been published. A planar format has two main advantages over beads in this context. First, beads are susceptible to motion during readout unless immobilized. Second, the shape of the bead requires that more complex procedures be used to remove the fluorescent background and determine the intensity arising over the entire volume of the bead.

Fluorometric microvolume assay technology (FMAT) was used as a detection method in FLISA bead-based homogenous assays for high-throughput screening. The optical system of FMAT has been described in detail[11,35] and a commercial FMAT scanner was released[11] in 1999. The FMAT system consisted of a confocal scanner with a $20\times$ NA 0.45 objective for detecting the FLISA with 6-μm-diam polystyrene beads in a homogenous immunoassay format.

Confocal readout of microarray format immunoassays was accomplished previously and there are commercially available scanners for this purpose.[36,37] The requirement when using such a confocal microscope system for microarray scanning is a very flat surface for the microarray substrate and sufficient scanning speed to avoid photobleaching of the fluorophores.[38] There is, however, no consensus on the benefits of confocal readout in the literature. For example, confocal readout has been presented as a sensitive method for determination of fluorescent signals emitted from the spots while rejecting out-of-focus background.[3] Conversely, it has been argued that most of the background signal on microarrays comes from nonspecific binding to the slide surface, which is in the same plane of focus as the sample and, thus, confocal read out provides little benefit as a microarray scanning method.[38]

Two-photon excitation has been described as another optical sectioning method for measuring the degree of binding of a fluorescent tracer attached to 3-μm polystyrene microparticles in a homogeneous immunoassay.[39] An instrument for two-photon excitation microparticle fluorometry (TPX) was built to detect the fluorescence from individual microparticles (1 to 10 μm) in suspension and measure C-reactive protein,[40] antiadenovirus antibodies,[41] and influenza A and B virus antigens.[42] The authors reported good sensitivity and dynamic range with no washing steps along with the ability to multiplex the assay. Real-time monitoring of the bioreaction and testing of the plasma samples demonstrated the potential of the TPX method for development of clinical immunoassays.[40]

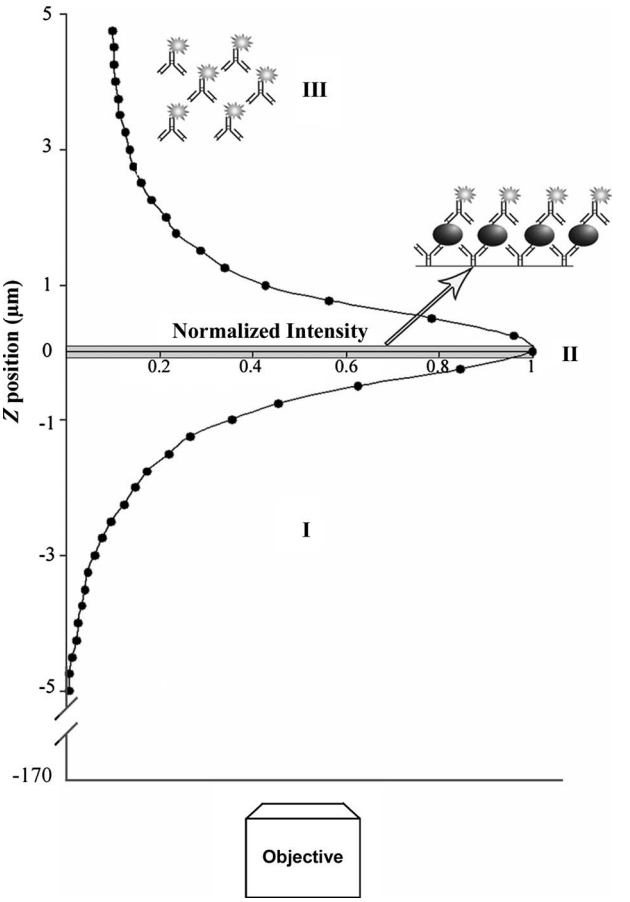

Fig. 1 Schematic diagram of a confocal sandwich immunoassay. The response curve has three zones: (I) the negative z position represents locations inside the ~170-μm-thick glass slide; (II) the location of the thin sandwich immunoassay film (~50 nm thick); and (III) the positive z position shows the fluorescent overlayer of unbound secondary antibody. The assay structure consisting of overlayer, thin film, and glass substrate is located above the objective and inverted microscope. To clarify the geometry of the assay with respect to the microscope the graph is oriented relative to the laboratory axes. Subsequent figures plot axial position horizontally.

Here we demonstrate a set of planar FLISA assays requiring optical sectioning to read out. The assays are based on a model sandwich immunoassay consisting of a goat antihuman immunoglobulin G (IgG) immobilized on a glass surface and a goat FITC-labeled antihuman IgG, which are used to detect human IgG. The model system was used to explore the confocal readout process while carrying it out in a spectrum of assays ranging from completely heterogeneous (two wash steps) to completely homogeneous (no wash steps). In these model systems, confocal readout enables fewer wash and incubation steps compared to conventional planar assays. By eliminating wash steps, the confocal assay is simpler and potentially more rapid.

1.1 *Theory*

1.1.1 *Optically sectioned detection of planar format immunoassays*

The key part of the confocal sandwich immunoassay (Fig. 1) is a fluorescent layer consisting of three stacked IgG mol-

ecules, which is <50 nm in thickness.[43–45] Depending on the orientation of the IgGs within the film, the thickness may range from ~12 to 45 nm. This dimension varies depending on whether it is estimated based on x-ray crystallographic data, scanning probe micrsocpy, or electron microscopy.[42–45] The value of 50 nm used here is meant to be a conservative estimate indicating that the film thickness is arbitrarily thin under the measurement conditions. In contrast to beads, the axial position of a planar thin fluorescent film oriented along the bottom of a plate can not be detected with a conventional microscope. Hence, there is no way to determine the location and relative intensities of the thin film and overlayer with such a system. In addition, the thickness of this thin fluorescent layer is below the resolution limit of all but the most advanced far-field fluorescence microscopes.[46] Although the thickness of IgGs stacked in a film can not be measured with a confocal microscope due to the diffraction limit, both the position on the maximum in the axial response curve and the intensity of light from the film can be measured with considerable precision.

In the confocal microscope, the planar assay format can be thought of as the sum of a thin film and an overlayer. An optical model of this system consists of a 50-nm thin film and a uniformly fluorescent overlayer beginning 50 nm above the glass surface and extending away from the film (Fig. 1). The thin film and overlayer differ only in the concentration-dependent intensity, designated C_1 and C_2, respectively. More rigorously, the two fluorescent objects (O) in the microscope can be given as a function of position along the z axis: $O_1(z)=C_1$ for $0<z<50$ nm and is 0 everywhere else, and $O_2(z)=C_2$ for 50 nm$\leqslant z<\infty$ and is 0 elsewhere. The overall object function is the sum of the two:

$$O(z) = O_1(z) + O_2(z). \tag{1}$$

For the purpose of the assay, the key to making accurate measurements of surface-bound fluorescence is the ability to selectively determine the concentration-dependent intensities C_1 and C_2.

In the microscope, the object function is not observed directly. Instead, the measured object (M) depends on the object function convolved with **h**, the confocal point spread function (PSF):

$$M(z) = \mathbf{h} \otimes O(z). \tag{2}$$

Since the diffraction-limited resolution along the z axis in a confocal microscope observed at a high NA is of the order of 500 nm, the surface-bound film is thin relative to the resolution of the microscope. This has the consequence that although the object as modeled consists of exclusive zones associated with either C_1 or C_2, the measured z axis "image" contains signals arising from both the overlayer and the thin film at every position along the z axis. For large z, the contribution of the film can be made arbitrarily small. A similar condition does not hold for the overlayer; the overlayer will contribute significantly to the signal at all locations along z due to blurring by the confocal PSF. Note that M can be broken down into the parts corresponding to the two composing objects:

$$M(z) = \mathbf{h} \otimes O_1(z) + \mathbf{h} \otimes O_2(z). \tag{3}$$

This equation suggests two ways to obtain information selectively from the thin film. The first approach is to convolve ideal objects [Eqs. (1) and (2)] with a computed PSF. For this study, the PSF, as described by van der Woort and Brakenhoff,[47] was applied to idealized objects, as in Eq. (1). The relative intensities associated with C_1 and C_2 are then adjusted until a best fit to the measured data is obtained using least-squares minimization. Alternately, a semiempirical approach can be used in which the axial response of the microscope is measured for a thin film in the absence of an overlayer and for the overlayer in the absence of the thin film. The measured data are then synthesized by making linear combinations of the two measured objects. The best results are obtained by fitting the observed data to simplified functions that mimic much of the behavior of planar objects modified by PSFs. The Cauchy-Lorentz function and the cumulative Cauchy-Lorentz function are comparatively simple functions that fit the shape of real axial response functions affected by aberrations reasonably well. The semiempirical fit used the following form:

$$M(z) = C_1 \frac{1}{\pi\gamma\{1+[(z-z_0)/\gamma]^2\}} + C_2\left[\frac{1}{\pi}\arctan\left(\frac{z-z_0}{\gamma}\right)+\frac{1}{2}\right] + B, \tag{4}$$

where z is the axial position, z_0 is the center of the thin film, γ is the width of the response, and B is a constant that corrects for electronic offsets and photomultiplier tube background in the confocal microscope.

1.1.2 *Adsorption of proteins to a solid phase*

The Langmuir equation is widely used to describe equilibrium adsorption phenomena.[3,48] The Langmuir isotherm was originally developed to model the adsorption of gas molecules to solid phases but it has been further applied to the adsorption of proteins to a solid phase[49] as follows:

$$F = \frac{F_{\max}[C]}{K_D + [C]}. \tag{5}$$

In this equation, F is the observed fluorescence, $F_{\max}$ is the maximal fluorescence, $[C]$ the concentration of protein in the solution, and K_D is the thermodynamic dissociation constant.

1.1.3 *Estimating errors in parameters*

Numerical differentiation can be used to estimate errors in parameters found by least-squares minimization[50] [e.g., least squares fits to Eq. (4)]. The standard deviations s_i of the i'th parameter a_i is

$$s_i = \left[\mathbf{P}^{-1}_{i,i} * \left(\frac{ss_{\text{resid}}}{n-k}\right)\right]^{1/2}. \tag{6}$$

The treatment here is substantially based on Billo.[50] This reference should be consulted for further details of the method. In Eq. (6) $\mathbf{P}^{-1}_{i,i}$ is the i'th diagonal element of the inverse of the matrix $\mathbf{P}$, ss_{resid} is the residual sum of squares for the model, n is the number of data points, and k is the number of parameters; $\mathbf{P}$ has elements given by

$$\mathbf{P}_{i,j} = \sum_{n=1}^{N} \frac{\delta M}{\delta a_i} \frac{\delta M}{\delta a_j}, \tag{7}$$

where $\delta M/\delta a_i$ and $\delta M/\delta a_j$ are partial derivatives of the model function [e.g., Eq. (4)] with respect to the i'th and j'th parameters. The derivatives can be approximated as $\Delta M/\Delta a_i$ by making small changes in a coefficient and computing the change in M. In this fashion, the elements of $\mathbf{P}$ are computed. We compute $\mathbf{P}^{-1}$ to estimate the errors in the estimated parameters.

2 Materials and Methods

2.1 *Reagents*

Human IgG (Product No. I4506), goat antihuman IgG (γ-chain specific) (Product No. I3382), goat antihuman IgG (γ-chain specific), FITC conjugate (Product No. F-0132), bovine serum albumin (BSA) minimum 98% (Product No. A7030), Dulbecco's phosphate-buffered saline (PBS) pH 7.4 (Product No. D8537), and NaN_3 (Product No. S8032) were purchased from Sigma-Aldrich Company Ltd. (Dorset, United Kingdom). The step size optimization study employed quantum dot labeled goat $F(ab')_2$ anti-human IgG (Product No. Q11231MP; Invitrogen Ltd.; Paisley, United Kingdom). Chambered cover glass slides (Lab-Tek chambered #1.0 borosilicate, Product No. 155411, Nalgene Nunc International, United States) and glass bottom 96-well plates (Product No. 164588, Nalgene Nunc International, United States) were used as solid supports for the immunoassay.

2.2 *Instrumentation*

A confocal scanner head (TCS NT; Leica Microsystems, Heidelberg GmbH, Germany) installed on an inverted microscope (DMIRBE, Leica Microsystems Wetzlar GmbH, Germany) was used for the optical sectioning of the immunoassay. The 488-nm line of an argon ion laser was used for excitation and the emission fluorescent intensity was detected using a 530/30-nm bandpass filter. The objectives used were HC PL FLUOTAR 10×0.3 DRY, PL FLUOTAR 16×0.5 IMM, HCX PL FL L 40×0.6 CORR, HCX PL FLUOTAR L 40×0.75 DRY, and HCX PL FLUOTAR L 63×0.7 CORR.

2.3 *Preparation of Confocal Sandwich Immunoassay*

The IgG immunoassays were conducted by immobilizing antihuman IgG as the capture antibody on chamber slides or 96-well plates overnight at 4 °C. The remaining sites for protein binding were blocked with a solution of 1% BSA (1% BSA in PBS with 0.02% NaN_3) for 2 h. After washing with PBS, for heterogeneous immunoassay, human IgG was added as an antigen and incubated for 2 h with shaking. The chambers/wells were washed with buffer. Goat anti-human IgG-FITC was added to the chambers/wells as the secondary labeled antibody and incubated for 1 h. For the homogenous format assays, human IgG and goat antihuman IgG-FITC were added simultaneously to the chambers/wells and incubated for 3 h. All steps from blocking to final incubation were performed at room temperature under continuous shaking. The chambers/plates were scanned with the confocal microscope without washing the second labeled antibody. The chambers/wells were then washed after scanning to investigate the effect of washing the secondary antibody on the response of the immunoassays.

2.4 *Analysis*

The sum of the intensity of each image in the stack of confocal images was computed and plotted against z axis position. These data were fit to Eqs. (2) and (4) using least-squares minimization. Detection limits were determined in two steps. First, the dose response curve was determined over a range of antigen concentration from 0 to 500 ng/ml with three replicates at each concentration. This was used to determine the slope of the linear portion of the response curve. Second, a further 10 replicates at the lowest detectable concentration from the dose response curve and the blank were measured and used to calculate the detection limit (DL):

$$\mathrm{DL} = \frac{ts}{m}, \tag{8}$$

where m is the slope of the linear portion of a dose response curve, $t=2.821$, and s is the standard deviation of a set of 10 sample measurements. Reported "lowest detected concentrations" represent the lowest concentration of the sample generating a significant ($p<0.05$) difference from a set of blank measurements based on a t test.

3 Results

3.1 *Quality Assessment of Parameters Affecting the Confocal Axial Response*

Image quality is important when evaluating the performance of a confocal microscope.[51–53] We investigated parameters affecting the quality of the response from the confocal microscope relevant to our assays: NA, pinhole size, and step size. Step size is discussed in Sec. 3.2.3.

3.1.1 *NA*

The intensity of a thin fluorescent film resulting from the human IgG model system after removal of the overlayer was measured in the confocal microscope with five different objectives varying in NA from 0.3 to 0.7 in a 512×512 region. The axial response was measured with a 74-μm pinhole every 0.4 μm along the z axis for a total of 50 images. While remaining constant in this set of experiments, the pinhole was below one Airy disk diameter and has little or no effect on the resolution for this set of magnifications and NAs. The full width at half maximum (FWHM) was measured for each objective (Table 1). As expected, the FWHM decreased with increasing NA with all the objectives showing an axial response to the thin film even at low NA. The improved resolution at a high NA is advantageous as it will result in less blurring between film and overlayer and thus improve both sensitivity and limits of detection. Based on these results, the $40\times$NA 0.75 objective was selected for subsequent use.

3.1.2 *Pinhole size*

The effect of the pinhole size on the intensity and resolution of the axial response was studied using the $40\times$NA 0.75 objective using 50 steps of 0.4 μm along the z axis. The

Table 1 Variation of the FWHM of the axial response to a thin film when observed in the microscope as a function of NA for a variety of objectives.

Objective	FWHM (μm)
10×NA 0.30	10.5
16×NA 0.5	7.0
40×NA 0.60	3.4
63×NA 0.70	2.8
40×NA 0.75	1.8

intensity of the signal increased nearly linearly with the pinhole size, but the FWHM of the axial response increased rapidly when the pinhole exceeded 150 μm (Fig. 2). The Airy disk diameter in the focal plane for the 40×NA 0.75 objective is approximately 140 μm and the optimal pinhole size is considered to be about 50 to 60% of this value,[53] in good agreement with the measured data. In addition, since the axial resolution does not improve significantly below this optimum, there is no benefit to further reduction in pinhole size. The only effect would be to reduce the signal strength from the film. Based on these experiments the pinhole size was set to 74 μm in subsequent experiments.

3.2 *Heterogenous Confocal Sandwich Assay*

3.2.1 *Response of film and overlayer*

Human IgG as the antigen (1 μg/ml) was added to coated chamber slides with the primary antibody (20 μg/ml) followed by the secondary antibody (40 μg/ml). The chamber was scanned in the confocal microscope using the 40×NA 0.75 objective using 50 steps of 0.2 μm along the z axis and a 74-μm pinhole without removing the fluorescent solution. The axial response exhibited three distinct features (Fig. 1): (I) a region of gradually decreasing signal trending to zero corresponding to the glass surface below the assay (0 to −5 μm), (II) a prominent peak arising from the thin film of concentrated fluorescence on the glass surface (0 μm), and (III) a region of decreasing fluorescence trending to a constant value resulting from the fluorescence of the overlayer of unbound secondary antibody (0 to 5 μm). The FWHM of the peak was 1.75 μm and the measured axial response indicated that the peak height contains signals from both the thin film and the fluorescent overlayer. The presence of overlayer fluorescence indicates that an excess of secondary antibody is present and must be separated from the film signal.

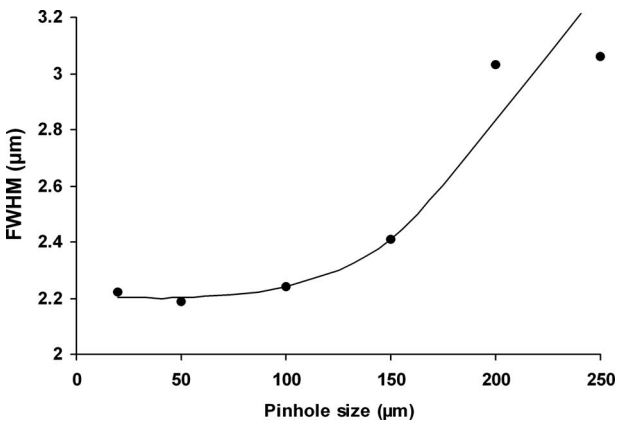

Fig. 2 Variation of the FWHM of the axial response of a confocal microscope as a function of pinhole size for the 40×NA 0.75 objective. The axial response begins to degrade when the pinhole is near the diameter of the Airy disk (~140 μm). The line is only to guide the eye.

3.2.2 *Decomposition of the signals of the thin film from an overlying fluorescent solution*

The first approach to separating the signals used full numerical simulation of the response from an object consisting of a thin film and overlayer convolved with a confocal PSF. The PSF was generated according to van der Voort and Brakenhoff;[47] however, the correspondence between experimental results and simulation was poor (data not shown), particularly in the wings of the thin film response. We ascribe this to aberrations resulting from refractive index mismatches (air, glass, and water) and the imperfect behavior of the lenses in our system.

The second method used for separation was based on distribution functions. Axial responses of the thin film in the absence of overlayer (a sample after washing the overlayer) and the overlayer in the absence of the thin film (a blank with same concentrations of first and secondary antibodies) were scanned [Fig 3(a)]. After testing the Gaussian and the Cauchy-Lorentz functions, the Cauchy-Lorentz functions were found to fit the measured data well. The sum of the Cauchy-Lorentz and cumulative Cauchy-Lorentz functions [Eq. (4)] fit well to the experimental data from the confocal immunoassay. This enabled the decomposition of the axial response of the assay into two objects: the thin film and the overlayer [Fig. 3(b)]. Excellent reproducibility ($\pm$0.04 μm) was seen in localizing the position of the thin film across the bottom of a chambered glass slide, indicating good slide flatness and microscope stability.

3.2.3 *Step size optimization*

The effect of step size on the separation of signals from the thin film and the fluorescent overlayer was studied by changing the step size in 0.1-μm intervals between 1.6 and 0.1 μm over an approximately 10-μm scan range with a 40×NA 0.75 objective. Where 10 μm was not evenly divisible by the step size the closest scan range to 10 μm was selected. This experiment was performed using quantum dots as the reporter fluorophore to mitigate photobleaching problems in repeated scans of the same location encountered with FITC-labeled materials. The results showed that the signal-to-noise ratio (SNR) of the thin film intensity parameter [C_1 in Eq. (4)] decreases in a logarithmic fashion as the step size increased (Fig. 4) with a tendency to overestimate the intensity of the thin film at step sizes $\geq$1 μm. Experiments described in subsequent portions of this report were performed using a 0.2-μm step size, which corresponded to an SNR of 168 in the optimization study.

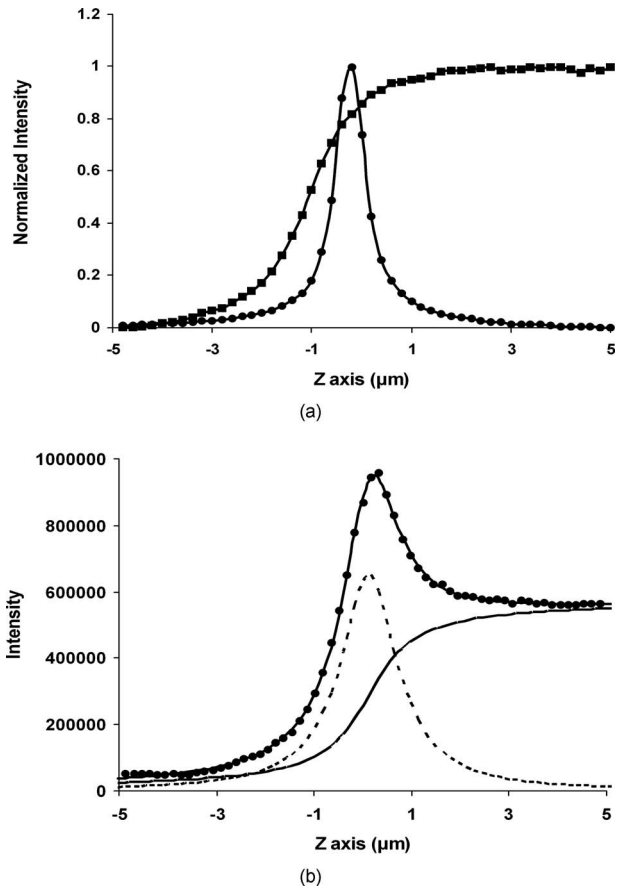

Fig. 3 Decomposition the signal of confocal immunoassay to the thin film and overlayer based on Cauchy-Lorentz function: (a) the axial responses of thin film (●) and overlayer (■) measured separately, and (b) the axial response of a sandwich immunoassay where the experimental data (●) is decomposed to thin film (- - -) and overlayer (—) after fitting the experimental data to the sum of thin film and overlayer. The line connecting the data points is the best fit to Eq. (4) for this set of measurements.

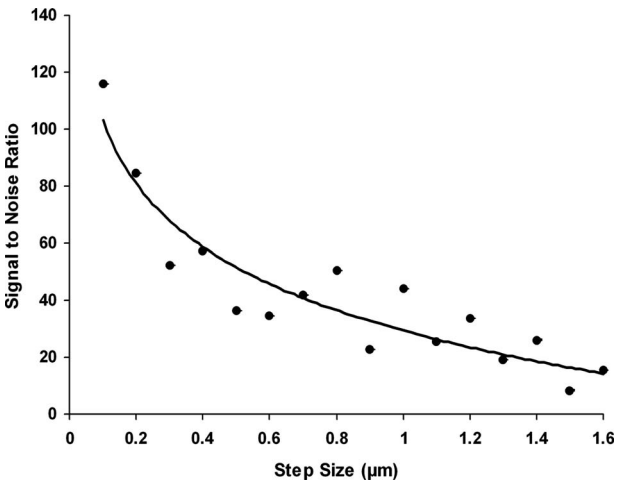

Fig. 4 Variation in SNR as step size increases over a fixed *z* axis scan range. Scans were done using a quantum dot reporter in this experiment to enable repeated scans of the same location to be comparable. All other data reported in this paper used FITC-labeled materials. The line shown corresponds to a logarithmic fit to the measured data. SNR improves as the step size decreases for a fixed scan range. This arises from better sampling of the axial response and an increase in the number of data points in the fit.

3.2.4 *Heterogenous confocal sandwich assay optimization*

We optimized the different steps of the immunoassay procedure for the widest dynamic range. The concentration of coating antibody (goat antihuman IgG) was tested from 2.5 to 320 μg/ml at a constant saturating level of antigen and secondary antibody (100 μg/ml) [Fig. 5(a)]. Using our protocol, the observed behavior appeared to follow a Langmuir adsorption process. A concentration of 160 μg/ml was chosen as optimal for the first antibody. This is a relatively high loading of the first antibody, but was found to work well for the chamber slides, reagents, and conditions in these experiments. The influence of the FITC-conjugated secondary antibody was investigated between 10 and 100 μg/ml [Fig. 5(b)] at a constant coating of antibody and the antigen yielding an optimal concentration of secondary antibody (50 μg/ml).

3.2.5 *Heterogeneous confocal planar immunoassay detection limit*

A glass 96-well plate was coated with a saturating concentration of primary antibody overnight. After blocking and washing the wells, serial dilutions of human IgG over the range from 0.5 μg/ml to 0.5 ng/ml, and the same volume of buffer with no human IgG as blank were added to the wells and detected with a low concentration of secondary antibody (0.5 μg/ml). Figure 6(a) shows the calibration curve plotted as the difference between intensity of sample and the average of blank signal ($n=3$) versus antigen concentration. The wells were washed with PBS and scanned again to see the effect of washing on responses. The dose response curve before washing the overlayer has a good linear range over the studied range of human IgG concentrations ($r^2=0.9984$). A comparison of average intensities of the low concentrations of antigen and blanks ($n=10$) showed that 5 ng/ml (before washing) and 10 ng/ml (after washing) of human IgG could be detected with >98/% confidence. The confidence level reported is from a two-tailed test. Strictly speaking, a one-tailed test can be used as the only relevant result is when the average blank is less than the sample. We chose to report the confidence level of the more conservative test. The calculated detection limits were 5.5 (before washing) and 10.4 ng/ml (after washing). The protocol with fewer wash and incubation steps was more sensitive, an effect we ascribe to some second antibody being rinsed from the surface.

3.3 *Homogeneous Confocally Detected Planar Immunoassay*

To demonstrate the adaptability of the confocally detected immunoassay to a homogenous format, the same model system was adopted to remove all sample and detection wash steps. A serial dilution of antigen over a range from 0.5 μg/ml to 0.5 ng/ml was compared to blanks consisting of PBS buffer with no human IgG. A low concentration of second antibody (0.5 μg/ml) was added simultaneously with the prepared antigen solution to the wells of a 96-well plate coated with a saturating amount of primary antibody. The dy-

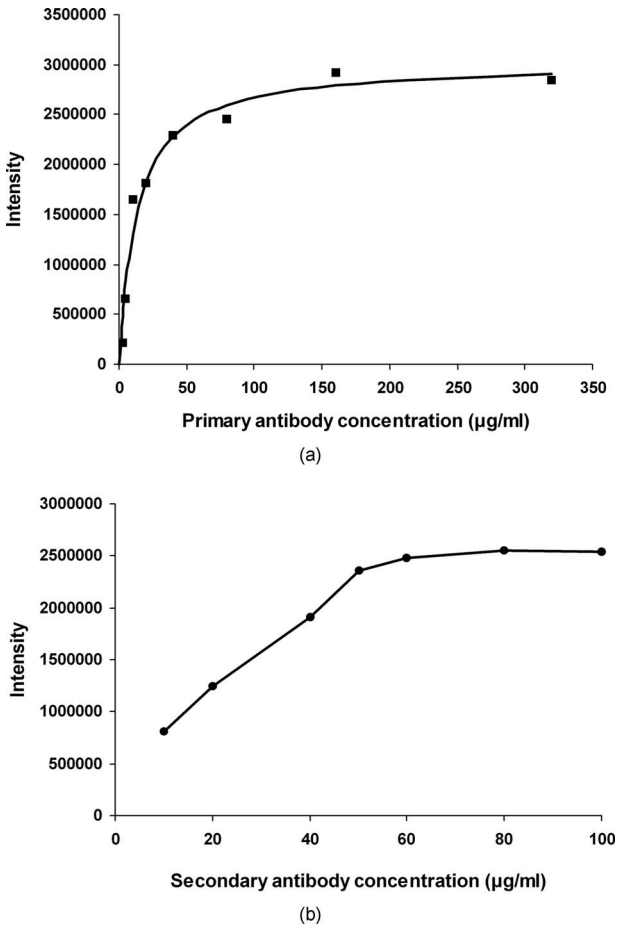

Fig. 5 Optimization of the model assay system for wide dynamic range: (a) response curve of the primary antibody with Langmuir fit and (b) response curve of the secondary antibody.

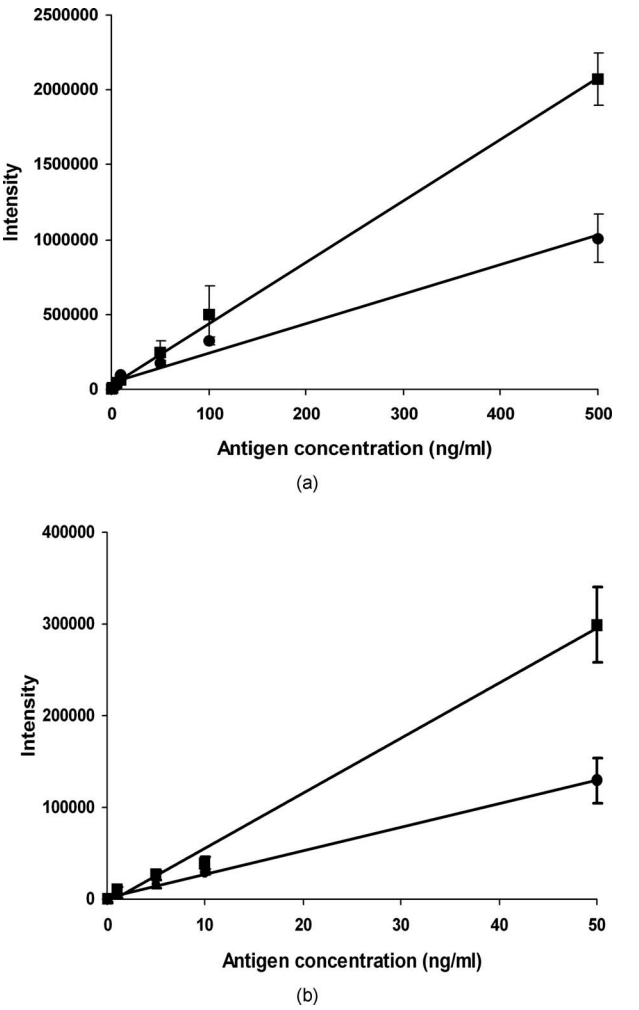

Fig. 6 Calibration curves of low concentrations of antigen before (■) and after (●) washing the fluorescent overlayer in (a) heterogeneous and (b) homogeneous format assays. The intensity was obtained after subtraction of the mean blank signal (n=10). Error bars correspond to $\pm s$ (n=3).

namic range of the calibration curve is shown in Fig. 6(b). The homogeneous format approached saturation around 0.5 μg/ml, a result consistent with the amount of second antibody (0.5 μg/ml) and the ratio of antigen and antibody molecular weights ($\sim$1:1). The dynamic range of the calibration curve was limited because the concentration of second antibody was intentionally kept low as this was found to improve sensitivity. The assays were subsequently washed for comparison purposes to evaluate the effect of washing on the thin film. The homogeneous assay detection limit was 2.2 ng/ml in the absence of all wash steps. As observed in the heterogenous assay results, the detection limit increased to 6.0 ng/ml after washing the overlayer. This reinforces the conclusion that wash steps remove analytically important material from the surface and the confocally detected homogeneous planer assay showed better detection limits than the heterogeneous one.

4 Discussion

We demonstrated a confocal readout method for detection of sandwich immunoassays using a human IgG model system. The response of the confocal system showed an antigen-dependent intensity variation originating from a thin film on a glass surface in the presence of an overlayer. We studied the axial response of the thin films generated by our assay to changes of NA and pinhole size and the results showed general agreement with published data on thin films.[27] These results are general to a wide range of planar format assay systems,[54,55] which could be readily adapted to become homogenous assays. These include planar arrays for the detection of genetic material and infectious diseases and many assays currently used in high-throughput screening. Further, other optical sectioning methods, such as two- and three-photon excitation and stimulated emission depletion (STED) could be used to similar or better effect to the standard confocal methods used here. Also, using high-speed confocal microscopy systems[24–30] will improve the slow frame rate of currently available confocal systems.

The consistent trend for improved detection limits observed as the number of wash steps decreased across all of the assay formats implies that weak antigen-dependent interactions were removed by washing. A related trend was seen when comparing the heterogeneous and homogeneous formats. Perhaps uniquely, the homogeneous format reported

here exhibited better sensitivity than any of the others. This is due to a combination of preserving interactions between the first antibody and the antigen, between the antigen and the second antibody, and possibly some formation of aggregates in solution between the antigen and the second antibodies prior to binding to the plate. By deleting all washing steps, it is possible to keep and detect even weak interactions between antigen and antibodies and improving the detection limits. Our 2.3-ng/ml detection limit for the human IgG immunoassay is competitive with others reported for this model system. For example, such a model system detected using quantum dots after removing the overlayer was[37] sensitive to 2 μg/ml. Note that the conditions producing the greatest sensitivity differ greatly from those producing a quantitative response over the widest dynamic range. Sensitivity is expected to be fundamentally limited by the Poisson statistics of photons generated by the overlayer. Therefore, sensitivity is enhanced at lower concentrations of secondary antibody because it lowers the noise generated by the overlayer. The widest dynamic range is produced by levels of secondary antibody sufficient to detect saturating levels of antigen. We anticipate future improvements in the method by optimized instrumentation, the introduction of quantum dots for better photostability,[56] higher NA optics, and additional optimization of the reagent and support surfaces.

A wide range of reports of confocal scanners for readout of fluorescent spots in planar arrays and bead assay systems have appeared in the literature. Despite numerous reports, we are not aware of a paper in which instrumental details are provided for the confocal scanner sufficient to reproduce the experiment together with a measured axial response from an immunoassay. Miriglia et al.[11] are exceptional in providing the NA and other optical details of their experiment. More common are reports of "proprietary" systems with few other details.[57,58] It is also of interest that, to our knowledge, none of these previous studies required a confocal or optically sectioned readout and the confocal readout was of arguable benefit. This work is an attempt to provide a clear example where the confocal readout is required and provides benefit (e.g., no wash steps and preservation of weak interactions) together with sufficient optical detail to determine how to best take advantage of optical sectioning in assays.

Our approach to planar assays shares advantages with other related homogenous and fluorescence-based assays and presents several attractive features. First, compared to conventional ELISAs, the planar homogenous assay could potentially save time due to the reduction of wash steps and the fluorescence readout does not require time for an enzyme reaction to develop. Second, assays can be stored for several days before readout.[59] Third, the planar homogeneous assay does not require beads or specialized reagents beyond those commonly available in many laboratories and will not suffer from bead motion during readout. Fourth, Due to the ability to eliminate wash steps, the approach is quite attractive for assays based on weaker interactions; such interactions are of very wide interest in high-throughput screening. High-throughput screening instrumentation already exists for confocally detected cellular assays and could be adapted for other types of screening and use in clinical labs. Fifth, since no washing is required, antigen-antibody reactions can be monitored in real time by measuring the intensity of the thin layer on the well bottom in the presence of free labeled antibody in the overlayer at any time. Evaluation of the rate constants of antigen–antibody pairs is possible under true assay conditions. Similar studies have been done on microparticles,[60] but not in planar formats. Studies on the kinetics of surface interactions by our method are underway. Sixth, it enables assays to be stacked in 3-D arrays followed optically sectioned readout. Finally, although we implemented the planar format using antibody-antigen interactions, the approach is general to a wide range of assays that can be presented as a reaction between a surface-bound species and free ligands.

The optical system is designed to work in chamber slides or multiwell plates presenting an optical glass surface with standard refractive index ($n=1.515$) and thickness (0.17 mm). This matches the design criteria for many microscope objectives and minimizes the spherical aberration due to refractive index mismatch. The use of different optical media could result in poor resolution and decreased intensity. For example, when working with polystyrene ($n=1.5917$) or polycarbonate ($n=1.5849$) plates, objectives with a correction collar for variable glass thickness (e.g., 0 to 2 mm) can be used to correct the lack of correct refractive index matching. The use of air objectives, as described here, simplifies sample-changing automation in an inverted geometry by eliminating immersion fluids.

The best separation between film and overlayer was achieved with the highest NA. Further improvement is expected at a higher NA due to better resolution and consequential improvements in detection limits, and better sensitivity are expected under these conditions. Practically, air lenses with longer working distances may be preferable; however, this choice is an engineering related compromise not a fundamental issue. Immersion objectives are somewhat awkward to use in inverted geometries. Finally, for a given a fixed scan range, SNR is improved by decreasing the step size.

Acknowledgments

This work was funded by the European Union Sixth Framework Programme as part of the FLUOROMAG consortium under Contract No. 037465. Dr. Yanzhou Zhou was funded by the Engineering and Physical Sciences Research Council (EPSRC) under a Life Sciences Interface Grant No. EP/E013422/1.

References

1. A. H. Wu, "A selected history and future of immunoassay development and applications in clinical chemistry," *Clin. Chim. Acta* **369**(2), 119–124 (2006).
2. C. P. Price and D. J. Newman, *Principles and Practice of Immunoassay*, Macmillan Reference Ltd., London (1997).
3. R. P. Ekins, "Ligand assays: from electrophoresis to miniaturized microarrays," *Clin. Chem.* **44**(9), 2015–2030 (1998).
4. G. Burns, A. Kurrle-Weittenhiller, J. Karl, W. D. Engel, A. Gromping, K. S. Boos, and D. Seidel, "A simple turbidimetric assay designed for the routine screening well as therapeutic monitoring of native LDL particles," *Clin. Chim. Acta* **303**(1–2), 155–165 (2001).
5. L. J. Lewellen and H. H. McCurdy, "A novel procedure for the analysis of drugs in whole-blood by homogeneous enzyme-immunoassay (emit)," *J. Anal. Toxicol.* **12**(5), 260–264 (1988).
6. D. A. Armbruster, E. C. Hubster, M. S. Kaufman, and M. K. Ramon, "Cloned enzyme donor immunoassay (cedia) for drugs-of-abuse screening," *Clin. Chem.* **41**(1), 92–98 (1995).
7. Z. S. Wu, S. B. Zhang, M. M. Guo, C. R. Chen, G. L. Shen, and R. Q. Yu, "Homogeneous, unmodified gold nanoparticle-based colori-

metric assay of hydrogen peroxide," *Anal. Chim. Acta* **584**(1), 122–128 (2007).
8. T. Kokko, L. Kokko, T. Soukka, and T. Lovgren, "Homogeneous noncompetitive bioaffinity assay based on fluorescence resonance energy transfer," *Anal. Chim. Acta* **585**(1), 120–125 (2007).
9. E. Loomans, A. M. van Doommalen, J. W. Y. Wat, and G. J. R. Zaman, "High-throughput screening with immobilized metal ion affinity-based fluorescence polarization detection, a homogeneous assay for protein kinases," *Assay Drug Develop. Technol.* **1**(3), 445–453 (2003).
10. E. F. Ullman, H. Kirakossian, A. C. Switchenko, J. Ishkanian, M. Ericson, C. A. Wartchow, M. Pirio, J. Pease, B. R. Irvin, S. Singh, R. Singh, R. Patel, A. Dafforn, D. Davalian, C. Skold, N. Kurn, and D. B. Wagner, "Luminescent oxygen channeling assay (LOCI(TM)): sensitive, broadly applicable homogeneous immunoassay method," *Clin. Chem.* **42**(9), 1518–1526 (1996).
11. S. Miraglia, E. E. Swartzman, J. Mellentin-Michelotti, L. Evangelista, C. Smith, I. Gunawan, K. Lohman, E. M. Goldberg, B. Manian, and P. M. Yuan, "Homogeneous cell- and bead-based assays for high throughput screening using fluorometric microvolume assay technology," *J. Biomol. Screening* **4**(4), 193–204 (1999).
12. J. H. Toney, A. Ogawa, M. Blair, and Y. W. Park, "A 'Mix and read' assay for insulin using fluorometric microvolume assay technology," *Assay Drug Develop. Technol.* **1**(4), 521–525 (2003).
13. E. E. Swartzman, S. J. Miraglia, J. Mellentin-Michelotti, L. Evangelista, and P. M. Yuan, "A homogeneous and multiplexed immunoassay for high-throughput screening using fluorometric microvolume assay technology," *Anal. Biochem.* **271**(2), 143–151 (1999).
14. D. K. Miller, J. D. Menke, N. S. Hayes, A. Uzieblo, D. Tew, Y. Hayashi, Y. F. Guan, A. Zhao, R. T. Cummings, Y. W. Park, and T. T. D. Yamin, "Development of a high-capacity homogeneous fluorescent assay for the measurement of leukotriene B-4," *Anal. Biochem.* **349**(1), 129–135 (2006).
15. M. Tanaka, K. Matsuo, M. Enomoto, and K. Mizuno, "A sol particle homogeneous immunoassay for measuring serum cystatin C," *Clin. Biochem.* **37**(1), 27–35 (2004).
16. J. H. W. Leuvering, B. C. Goverde, P. Thal, and A. Schuurs, "A homogeneous sol particle immunoassay for human chorionic-gonadotropin using monoclonal-antibodies," *J. Immunol. Methods* **60**(1–2), 9–23 (1983).
17. T. Aoki, S. Tsuchida, T. Yahara, and N. Hamaue, "Novel assays for proteases using green fluorescent protein-tagged substrate immobilized on a membrane disk," *Anal. Biochem.* **378**(2), 132–137 (2008).
18. T. Aoki, H. Kazama, M. Satoh, K. Mizuki, and H. Watabe, "A homogeneous assay for relative affinity of binding proteins using a green fluorescent protein tag and membrane disk," *Anal. Biochem.* **344**(1), 25–32 (2005).
19. A. Datti, R. S. Donovan, B. Korczak, and J. W. Dennis, "A homogeneous cell-based assay to identify N-linked carbohydrate processing inhibitors," *Anal. Biochem.* **280**(1), 137–142 (2000).
20. A. L. Niles, R. A. Moravec, P. E. Hesselberth, M. A. Scurria, W. J. Daily, and T. L. Riss, "A homogeneous assay to measure live and dead cells in the same sample by detecting different protease markers," *Anal. Biochem.* **366**(2), 197–206 (2007).
21. R. Lee, M. Tran, M. Nocerini, and M. Liang, "A high-throughput hybridoma selection method using fluorometric microvolume assay technology," *J. Biomol. Screening* **13**(3), 210–217 (2008).
22. X. Y. Xu, D. G. Georganopoulou, H. D. Hill, and C. A. Mirkin, "Homogeneous detection of nucleic acids based upon the light scattering properties of silver-coated nanoparticle probes," *Anal. Chem.* **79**(17), 6650–6654 (2007).
23. S. J. Wright and D. J. Wright, "Introduction to confocal microscopy," in *Method in Cell Biology*, pp. 2–81 Academic Press, San Diego (2002).
24. T. Wilson, R. Juskaitis, M. A. A. Neil, and M. Kozubek, "Confocal microscopy by aperture correlation," *Opt. Lett.* **21**(23), 1879–1881 (1996).
25. R. Wolleschensky, B. Zimmermann, and M. Kempe, "High-speed confocal fluorescence imaging with a novel line scanning microscope," *J. Biomed. Opt.* **11**(6), 064011 (2006).
26. P. J. Verveer, Q. S. Hanley, P. W. Verbeek, L. J. Van Vliet, and T. M. Jovin, "Theory of confocal fluorescence imaging in the programmable array microscope (PAM)," *J. Microsc.* **189**, 192–198 (1998).
27. Q. S. Hanley, P. J. Verveer, M. J. Gemkow, D. Arndt-Jovin, and T. M. Jovin, "An optical sectioning programmable array microscope implemented with a digital micromirror device," *J. Microsc.* **196**, 317–331 (1999).
28. T. Tanaami, S. Otsuki, N. Tomosada, Y. Kosugi, M. Shimizu, and H. Ishida, "High-speed 1-frame/ms scanning confocal microscope with a microlens and Nipkow disks," *Appl. Opt.* **41**(22), 4704–4708 (2002).
29. M. A. A. Neil, R. Juskaitis, and T. Wilson, "Method of obtaining optical sectioning by using structured light in a conventional microscope," *Opt. Lett.* **22**(24), 1905–1907 (1997).
30. D. Karadaglic and T. Wilson, "Image formation in structured illumination wide-field fluorescence microscopy," *Micron* **39**(7), 808–818 (2008).
31. J. Mellentin-Michelotti, L. T. Evangelista, E. E. Swartzman, S. J. Miraglia, W. E. Werner, and P. M. Yuan, "Determination of ligand binding affinities for endogenous seven-transmembrane receptors using fluorometric microvolume assay technology," *Anal. Biochem.* **272**(2), 182–190 (1999).
32. N. Komatsu, S. Shichijo, Y. Maeda, and K. Itoh, "Measurement of interferon-gamma by high-throughput fluorometric microvolume assay technology system," *J. Immunol. Methods* **263**(1–2), 169–176 (2002).
33. P. Zuck, Z. G. Lao, S. Skwish, J. F. Glickman, K. Yang, J. Burbaum, and J. Inglese, "Ligand-receptor binding measured by laser-scanning imaging," *Proc. Natl. Acad. Sci. U.S.A.* **96**(20), 11122–11127 (1999).
34. R. P. Ekins and F. W. Chu, "Multianalyte microspot immunoassay—microanalytical compact-disk of the future," *Clin. Chem.* **37**(11), 1955–1967 (1991).
35. L. J. Dietz, R. S. Dubrow, B. S. Manian, and N. L. Sizto, "Volumetric capillary cytometry: a new method for absolute cell enumeration," *Cytometry* **23**(3), 177–186 (1996).
36. T. Bacarese-Hamilton, L. Mezzasoma, A. Ardizzoni, F. Bistoni, and A. Crisanti, "Serodiagnosis of infectious diseases with antigen microarrays," *J. Appl. Microbiol.* **96**(1), 10–17 (2004).
37. B. Q. Sun, W. Z. Xie, G. S. Yi, D. P. Chen, Y. X. Zhou, and J. Cheng, "Microminiaturized immunoassays using quantum dots as fluorescent label by laser confocal scanning fluorescence detection," *J. Immunol. Methods* **249**(1–2), 85–89 (2001).
38. M. Schaferling and S. Nagl, "Optical technologies for the read out and quality control of DNA and protein microarrays," *Anal. Bioanal. Chem.* **385**(3), 500–517 (2006).
39. P. Hanninen, A. Soini, N. Meltola, J. Soini, J. Soukka, and E. Soini, "A new microvolume technique for bioaffinity assays using two-photon excitation," *Nat. Biotechnol.* **18**(5), 548–550 (2000).
40. M. E. Waris, N. J. Meltola, J. T. Soini, E. Soini, O. J. Peltola, and P. E. Hanninen, "Two-photon excitation fluorometric measurement of homogeneous microparticle immunoassay for C-reactive protein," *Anal. Biochem.* **309**(1), 67–74 (2002).
41. J. O. Koskinen, J. Vaarnor, R. Vainionpaa, and A. E. Soini, "A novel separation-free assay technique for serum antibodies using antibody bridging assay principle and two-photon excitation fluorometry," *Clin. Chim. Acta* **355**, S142–S142 (2005).
42. J. O. Koskinen, R. Vainionpää, N. J. Meltola, J. Soukka, P. E. Hänninen, and A. E. Soini, "Rapid method for the detection of influenza A and B virus antigens using TPX assay technique and dry-chemistry reagents," *J. Clin. Microbiol.* **45**, 3581–3588 (2007).
43. E. Cunningham and C. J. Campbell, "A novel self-assembled nanoparticulate film for covalent attachment of antibodies to plastic," *Langmuir* **19**(10), 4509–4511 (2003).
44. K. Wadu-Mesthrige, N. A. Amro, J. C. Garno, S. Xu, and G. Y. Liu, "Fabrication of nanometer-sized protein patterns using atomic force microscopy and selective immobilization," *Biophys. J.* **80**(4), 1891–1899 (2001).
45. F. R. F. Fan and A. J. Bard, "Imaging of biological macromolecules on mica in humid air by scanning electrochemical microscopy," *Proc. Natl. Acad. Sci. U.S.A.* **96**(25), 14222–14227 (1999).
46. G. Donnert, J. Keller, R. Medda, M. A. Andrei, S. O. Rizzoli, R. Lurmann, R. Jahn, C. Eggeling, and S. W. Hell, "Macromolecular-scale resolution in biological fluorescence microscopy," *Proc. Natl. Acad. Sci. U.S.A.* **103**(31), 11440–11445 (2006).
47. H. T. M. Vandervoort and G. J. Brakenhoff, "3-D image-formation in high-aperture fluorescence confocal microscopy—a numerical-analysis," *J. Microsc.* **158**, 43–54 (1990).
48. C. S. Lee, S. H. Lee, Y. G. Kim, J. H. Lee, Y. K. Kim, and B. G. Kim, "A method of binding kinetics of a ligand to micropatterned proteins on a microfluidic chip," *Biosens. Bioelectron.* **22**(6), 891–898 (2007).

49. A. P. G. A. W. Adamson, *Physical Chemistry of Surfaces*, Wiley, New York (1997).
50. E. J. Billo, *Excel for Chemists a Comprehensive Guide*, Wiley-VCY, New York (2001).
51. R. M. Zucker, "Evaluation of confocal microscopy system performance," *Methods Mol. Biol.* **319**, 77–135 (2006).
52. R. M. Zucker, "Quality assessment of confocal microscopy slide based systems: performance," *Cytometry* **69A**(7), 659–676 (2006).
53. J. B. E. Pawley, *Handbook of Biological Confocal Microscopy*, Springer, New York (2006).
54. J. S. Martinez, W. K. Grace, K. M. Grace, N. Hartman, and B. I. Swanson, "Pathogen detection using single mode planar optical waveguides," *J. Mater. Chem.* **15**(43), 4639–4647 (2005).
55. M. Pawlak, E. Schick, M. A. Bopp, M. J. Schneider, P. Oroszlan, and M. Ehrat, "Zeptosens' protein microarrays: a novel high performance microarray platform for low abundance protein analysis," *Proteomics* **2**(4), 383–393 (2002).
56. M. Seydack, "Nanoparticle labels in immunosensing using optical detection methods," *Biosens. Bioelectron.* **20**(12), 2454–2469 (2005).
57. L. Prix, P. Uciechowski, B. Bockmann, M. Giesing, and A. J. Schuetz, "Diagnostic biochip array for fast and sensitive detection of K-ras mutations in stool," *Clin. Chem.* **48**(3), 428–435 (2002).
58. V. Souplet, R. Desmet, and O. Melnyk, "Imaging of protein layers with an optical microscope for the characterization of peptide microarrays," *J. Pept. Sci.* **13**(7), 451–457 (2007).
59. Q. Gu, T. M. Sivanandam, and C. A. Kim, "Signal stability of Cy3 and Cy5 on antibody microarrays," *Proteome. Sci.* **4**, 21 (2006).
60. P. Hanninen, M. Waris, M. Kettunen, and E. Soini, "Reaction kinetics of a two-photon excitation microparticle based immunoassay-from modelling to practice," *Biophys. Chem.* **105**(1), 23–28 (2003).